

Transfer Learning for Deep-Unfolded Combinatorial Optimization Solver with Quantum Annealer

Ryo Hagiwara, Shunta Arai, and Satoshi Takabe
 Institute of Science Tokyo, Ookayama, Tokyo 152-8550, Japan
 (Dated: January 8, 2025)

Quantum annealing (QA) has attracted research interest as a sampler and combinatorial optimization problem (COP) solver. A recently proposed sampling-based solver for QA significantly reduces the required number of qubits, being capable of large COPs. In relation to this, a trainable sampling-based COP solver has been proposed that optimizes its internal parameters from a dataset by using a deep learning technique called deep unfolding. Although learning the internal parameters accelerates the convergence speed, the sampler in the trainable solver is restricted to using a classical sampler owing to the training cost. In this study, to utilize QA in the trainable solver, we propose classical-quantum transfer learning, where parameters are trained classically, and the trained parameters are used in the solver with QA. The results of numerical experiments demonstrate that the trainable quantum COP solver using classical-quantum transfer learning improves convergence speed and execution time over the original solver.

I. INTRODUCTION

A combinatorial optimization problem (COP) entails determining the minimum (or maximum) solution to an objective function with discrete variables under given constraints. Typical examples of COPs include the traveling salesman and knapsack problems. COPs are related to the P-NP problem, and in many cases, finding an optimal solution in polynomial time is considered difficult [1].

Two well-known optimization approaches are simulated annealing (SA) [2] and quantum annealing (QA) [3]. In particular, QA has attracted significant research attention owing to its ability to sometimes outperform classical optimization algorithms, such as SA, in terms of convergence speed and solution quality [4]. QA has been implemented in specialized devices, such as the quantum annealer [5]. However, the quantum annealer faces limitations such as a relatively small number of available qubits and fixed qubit couplings within the device. Mapping problem constraints onto the hardware's limited qubit connectivity of hardware often restricts the size and complexity of the instances that can be practically addressed [6–9].

To mitigate these limitations, a new sampling-based COP solver using gradient methods has been proposed [10], which we refer to as the Ohzeki method in this paper. In the Ohzeki method, a constrained problem is re-formulated as a sampling problem with auxiliary variables introduced by the Hubbard-Stratonovich transformation [11, 12]. Then, the method then iteratively executes two processes: a sampling process for the original variables and a gradient descent process for the auxiliary variables. This enables the quantum annealer to handle bigger problems by avoiding the costly mapping from constraints to a device. In addition, any sampler is applicable to the Ohzeki method, whereas the method was originally proposed for a quantum annealer. A drawback of the method is tuning step sizes in the gradient descent process. A heuristic selection of step sizes often leads to performance degradation.

In our previous study [13], we tuned the step sizes of the Ohzeki method in a *data-driven* manner. This concept in machine learning, known as deep unfolding (DU) [14, 15], uses techniques such as backpropagation to optimize the internal parameters of differentiable iterative algorithms. Because

DU is based on iterative algorithms, it provides an easy interpretation of the training parameters. Additionally, because only a few internal parameters must be learned, the learning costs are reduced. DU has been shown to improve convergence speed and approximation performance compared to the base algorithms [16]. Consequently, DU has been employed to develop novel optimization-based trainable algorithms for signal processing, including areas such as wireless communications [17], compressed sensing [18], and image processing [19]. For example, DU has been employed to handle COPs arising in wireless communication tasks such as digital signal detection, and DU has been employed for these detection algorithms, achieving remarkable performance improvements [17, 20]. In addition, some Deep-unfolded classical algorithms inspired by quantum computation have also been proposed [21, 22]. Overall, DU is a powerful model-based learning approach that improves existing algorithms.

In our previous work [13], we combined the Ohzeki method with DU to tune the step sizes, which affected the convergence speed and optimization performance. Specifically, automatic differentiation and backpropagation cannot be used when the learning step sizes. To circumvent this, we formulated a new learning strategy wherein a sampler estimates gradient information is approximated through a sampling part. We verified that the trainable solver, namely the deep-unfolded Ohzeki method (DUOM) was sufficiently trained using this strategy. In addition, DUOM accelerates the convergence of the original Ohzeki method with a constant step size, indicating the effectiveness of DU for a sampling-based algorithm. However, a limitation of this approach is the use of the classical Metropolis-Hastings (MH) algorithm [23, 24], rather than QA for sampling. This is inevitable because DUOM executes many times in the training process, and its training cost of DUOM with a quantum annealer is impractically high.

The aim of this paper is to propose and examine a learning strategy for DUOM with a quantum annealer to circumvent the costly training process. Specifically, we propose a *classical-quantum transfer learning* where the trainable parameters are preliminarily learned by DUOM with a classical sampler, and subsequently used to execute DUOM with a quantum annealer. We investigated the effect of a classical sampler on the training process by comparing the MH al-

gorithm with simulated quantum annealing (SQA) [25, 26], which emulates QA on a classical computer. We also compared the performance of the classical-quantum transfer learning with that of conventional parameter tuning by grid search. In addition, the execution time of DUOM with a quantum annealer was compared to that of a classical sampler to examine the quantum acceleration.

The remainder of this paper is organized as follows. Section II introduces the Ohzeki method for constrained binary quadratic optimization problems. Section III provides an overview of the DU and DUOM proposed in our previous study. Section IV describes classical-quantum transfer learning. Section V presents the results of numerical experiments conducted the performance of classical-quantum transfer learning. Finally, Section VI concludes the paper.

II. OHZEKI METHOD

To solve COPs using a quantum annealer, an optimization problem is converted into a quadratic unconstrained binary optimization (QUBO) format [27]. The penalty method is typically used when expressing a COP with linear constraints in QUBO form [27].

Consider the following QUBO with linear constraints

$$\begin{aligned} \min_{\mathbf{x} \in \{0,1\}^N} \quad & f_0(\mathbf{x}) \\ \text{s.t.} \quad & f_k(\mathbf{x}) = C_k \quad (k = 1, \dots, m), \end{aligned} \quad (1)$$

where $f_0(\mathbf{x})$ is the objective function representing the cost or energy to be minimized, and $f_k(\mathbf{x}) = C_k$ is the k -th constraints in which f_k is a linear function. This formulation can be used to express practical COPs such as the traveling salesman problem and the graph partitioning problem. To convert COP (1) into the QUBO form, the penalty method introduces the following loss function by adding a penalty term to the objective function $f_0(\mathbf{x})$:

$$L_\lambda(\mathbf{x}) = f_0(\mathbf{x}) + \lambda \sum_{k=1}^m (f_k(\mathbf{x}) - C_k)^2, \quad (2)$$

where $\lambda > 0$ is a hyperparameter controlling the penalty strength. If a solution satisfies the constraints of COP (1), the penalty term $\lambda \sum_{k=1}^m (f_k(\mathbf{x}) - C_k)^2$ in the loss function becomes zero.

Although this penalty method effectively converts COP (1) into the QUBO form, it also increases the number of qubits required for QA, placing an upper bound on the size of problems solvable by QA. That is, the number of quadratic terms in the QUBO increases, requiring additional qubits for minor embedding [6–9] to map logical variables onto the physical qubits of a quantum annealer.

To address this issue, Ohzeki proposed a solver [10] that uses the Hubbard-Stratonovich transformation [11, 12] to linearize the penalty terms. Let us consider solving the constrained COP (1) by sampling from the Boltzmann distribu-

Algorithm 1 Ohzeki method

```

1: Input:  $\beta, \lambda, f_0, \{f_k, C_k\}$ , max iteration:  $T$ 
2: Initialize:  $\mathbf{v}^{(0)} \in \mathbb{R}^m$ 
3: for  $t = 0, 1, \dots, T - 1$  do
4:   estimate  $\{\langle f_k(\mathbf{x}) \rangle_{Q(\mathbf{x}; \mathbf{v}^{(t)})}\}$  by sampling from
5:    $Q(\mathbf{x}; \mathbf{v}^{(t)}) \propto \exp(-\beta f_0(\mathbf{x}) + \beta \sum_{k=1}^m v_k^{(t)} f_k(\mathbf{x}))$ 
6:   update  $\mathbf{v}^{(t+1)}$  by
7:    $v_k^{(t+1)} = v_k^{(t)} + \eta_t (C_k - \langle f_k(\mathbf{x}) \rangle_{Q(\mathbf{x}; \mathbf{v}^{(t)})})$ 
8: end for
9: return  $\arg \min L(\mathbf{x}; \lambda)$  by sampling from  $Q(\mathbf{x}; \mathbf{v}^{(T)})$ 

```

tion corresponding to Eq. (2), defined by

$$Q(\mathbf{x}) = \frac{1}{Z} \exp \left(-\beta f_0(\mathbf{x}) - \beta \lambda \sum_{k=1}^m (f_k(\mathbf{x}) - C_k)^2 \right),$$

where β is the inverse temperature, which should be sufficiently large for optimization, and Z is the partition function. Alternatively, the Ohzeki method samples from a new Boltzmann distribution with auxiliary variables \mathbf{v} introduced by the Hubbard-Stratonovich transformation [10]. The distribution is given by

$$Q(\mathbf{x}; \mathbf{v}^{(t)}) = \frac{1}{Z(\mathbf{v}^{(t)})} \exp \left(-\beta f_0(\mathbf{x}) + \beta \sum_{k=1}^m v_k^{(t)} f_k(\mathbf{x}) \right). \quad (3)$$

A sampler is used to estimate the expectations $\{\langle f_k(\mathbf{x}) \rangle_{Q(\mathbf{x}; \mathbf{v}^{(t)})}\}_{k=1}^m$ of functions $\{f_k(\mathbf{x})\}_{k=1}^m$ over the distribution (3). Then, the auxiliary variables \mathbf{v} are updated to satisfy $\langle f_k(\mathbf{x}) \rangle_{Q(\mathbf{x}; \mathbf{v}^{(t)})} = C_k$ for each k . This is achieved by gradient descent with the following update rule for each k :

$$v_k^{(t+1)} = v_k^{(t)} + \eta_t (C_k - \langle f_k(\mathbf{x}) \rangle_{Q(\mathbf{x}; \mathbf{v}^{(t)})}) \quad (t = 0, 1, \dots), \quad (4)$$

where η_t the step size at iteration t for the gradient descent method.

Algorithm 1 presents the pseudocode of the Ohzeki method. Using this method, the number of required qubits is reduced, allowing a quantum annealer to handle larger constrained COPs.

III. DEEP-UNFOLDED OHZEKI METHOD

In this section, we briefly summarize the concept of DU. We then introduce the deep-unfolded Ohzeki method, wherein the internal parameters are learned in a data-driven manner.

A. Deep Unfolding

DU is a deep learning technique that optimizes internal parameters in iterative algorithms by embedding trainable variables and applying backpropagation. Here, we illustrate for gradient descent as an example. For interested readers, please refer to previous reviews [28, 29].

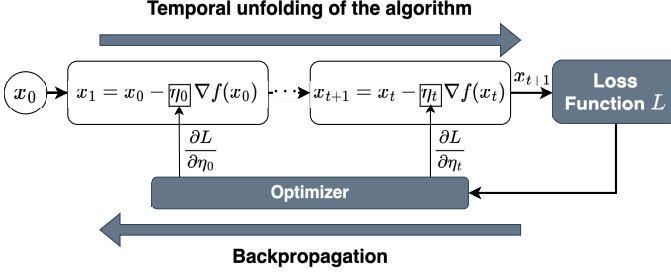


FIG. 1: A schematic diagram of deep-unfolded gradient descent (upper) and its training process (lower).

In gradient descent, the update rule for variable \mathbf{x} at iteration $t = 0, 1, \dots, T - 1$ is given by

$$\mathbf{x}_{t+1} = \mathbf{x}_t - \eta_t \nabla f(\mathbf{x}),$$

where T is the total number of iterations, η_t is a step size, and f is a random objective function, such as a quadratic function with random coefficients, to be minimized. The selection of an appropriate step size is crucial; an excessively large step size may result in failure to converge, whereas an overly small step size may result in slow convergence or cause the algorithm to fall into local minima. In DU, the iterative process is temporally unfolded, embedding trainable parameters to optimize performance. In this case, trainable step sizes $\{\eta_t\}_{t=0}^{T-1}$ are introduced as shown in Fig. 1.

Assume that a dataset $\{\mathbf{x}_0^{(d)}, f^{(d)}(\mathbf{x}), \mathbf{x}_*^{(d)}\}_{d=1}^D$ is available, where D represents the number of problem instances in the dataset. Each instance contains an initial point $\mathbf{x}_0^{(d)}$, an objective function $f^{(d)}(\mathbf{x})$, and corresponding optimal solution $\mathbf{x}_*^{(d)}$. This setting corresponds to supervised learning. To learn $\{\eta_t\}_{t=0}^{T-1}$ suitable for the dataset, a loss function L is introduced. For instance, the mean squared error (MSE) loss function is defined as

$$L = \frac{1}{D} \sum_{d=1}^D \|\mathbf{x}_T^{(d)} - \mathbf{x}_*^{(d)}\|_2^2, \quad (5)$$

where $\mathbf{x}_T^{(d)}$ is an output of a gradient descent with initial point $f^{(d)}(\mathbf{x})$. In other words, the loss function for DU minimizes the distance between the output obtained using a given trainable parameters and the optimal solutions. Then, using back-propagation, the gradients $\partial L / \partial \eta_t$ are calculated to find optimal step sizes that minimize the loss function. This learning process illustrated by the lower arrow in Fig. 1. As a result, the learned gradient descent accelerates convergence and improves approximation performance compared with that of the original gradient descent [30].

B. Deep-Unfolded Ohzeki Method

As mentioned previously, the Ohzeki method is an efficient COP solver that uses gradient descent. However, because the Ohzeki method applies gradient descent (4) to a

non-convex objective function, its convergence speed and performance depend on the step size, which is selected heuristically. To address this issue, the authors have proposed the deep-unfolded Ohzeki Method (DUOM) in [13], which learns step sizes based upon DU.

The learnable parameters in the DUOM are the step sizes $\{\eta_t\}_{t=0}^{T-1}$ in Eq. (4). The DUOM adjusts the step sizes to minimize the loss function (2), aiming to satisfy the constraints and minimize the objective function. Unlike the supervised learning described in the previous subsection, DUOM adopts *unsupervised learning* which does not require optimal solutions for a dataset. Unsupervised learning is suitable owing to the challenge of estimating optimal solutions for constrained COPs in advance. Then, the step sizes are updated using an optimizer such as Adam [31], with gradients obtained by backpropagation. The partial derivative of the loss function L_λ with respect to η_t is given by

$$\frac{\partial L_\lambda}{\partial \eta_t} = \sum_{k=1}^m \frac{\partial L}{\partial v_k^{(T)}} \left(\prod_{u=t+1}^{T-1} \frac{\partial v_k^{(u+1)}}{\partial v_k^{(u)}} \right) \frac{\partial v_k^{(t+1)}}{\partial \eta_t}, \quad (6)$$

$$\frac{\partial v_k^{(u+1)}}{\partial v_k^{(u)}} = 1 - \eta_u \frac{\partial \langle f_k(\mathbf{x}) \rangle_{Q(\mathbf{v}^{(u)})}}{\partial v_k^{(u)}}. \quad (7)$$

Because the expectation $\langle f_k(\mathbf{x}) \rangle_{Q(\mathbf{x}; \mathbf{v}^{(t)})}$ is estimated via non-differentiable sampling, automatic differentiation of deep-learning packages such as PyTorch [32] is inapplicable to Eq. (7). Although this gradient can be approximated by numerical differentiation, this is computationally expensive and inefficient as it requires additional sampling processes. As an alternative, in [13], the authors proposed the sampling-based gradient estimation via the variance. Using Eq. (3), we have

$$\frac{\partial \langle f_k(\mathbf{x}) \rangle_{Q(\mathbf{x}; \mathbf{v}^{(t)})}}{\partial v_k} = \beta \left(\langle f_k^2(\mathbf{x}) \rangle_{Q(\mathbf{x}; \mathbf{v}^{(t)})} - \langle f_k(\mathbf{x}) \rangle_{Q(\mathbf{x}; \mathbf{v}^{(t)})}^2 \right). \quad (8)$$

This allows for gradient estimation in the forward process. That is, the gradient is efficiently calculated using the variance, which approximated when sampling the expectation over $Q(\mathbf{x}; \mathbf{v}^{(t)})$.

In [13], the numerical results showed that DUOM exhibited excellent performance compared with that of the conventional Ohzeki method. However, DUOM could only be deployed with a classical sampler because the training process required a large number of sampling processes. In the numerical experiments on image reconstruction, the sampling process was executed approximately one million times during training. Although a quantum annealer is applicable to DUOM in principle, the use of QA in the training process is impractically expensive.

IV. CLASSICAL-QUANTUM TRANSFER LEARNING

The aim of this study is to examine DUOM using a quantum annealer without QA during the training process. The key observation is that any sampler is applicable to DUOM.

We propose classical-quantum transfer learning as a new learning strategy. In the scheme, in general, an unfolded algorithm is trained using a classical (approximate) algorithm, and

the learned parameters are then transferred to that with a quantum algorithm. Unlike conventional transfer learning, where a model trained on a given dataset is applied to another type of dataset, classical-quantum transfer learning uses classical computation in the training process and quantum computation in execution. The difference in algorithms between training and execution is considered to incur performance degradation, as the learned parameters may be unstable in quantum algorithms. However, if the difference is sufficiently small, the performance degradation can be reduced. This reflects the importance of selecting a classical algorithm for the training process.

In our case, classical-quantum transfer learning entails that the trained step sizes of DUOM with a classical sampler are transferred to DUOM with a quantum annealer. In particular, we examined the MH algorithm and SQA as classical samplers used for training. Figure 2 presents an overview of classical-quantum transfer learning. This approach significantly reduces costs by eliminating quantum computation during the training process.

It should be emphasized that the proposed classical-quantum transfer learning differs from other techniques developed in quantum computing. For example, the quantum approximate optimization algorithm (QAOA) [33] handles COPs by tuning the internal parameters related to the quantum gates. When the QAOA parameters are tuned, the objective function is evaluated by executing a quantum circuit multiple times. Classical Bayesian or gradient-based optimization, with gradients evaluated using the parameter shift method [34], is then used for parameter updates. The feedback loop between quantum circuit execution and classical optimization in QAOA differs from that in classical-quantum transfer learning, wherein the training process does not involve quantum computation. In other words, the QAOA parameter tuning process is not classical-quantum transfer learning because the parameter update depends on outputs of quantum computation. On the other hand, classical-quantum transfer learning does not involve quantum computation during the training process. Instead, the training is performed entirely on a classical computer, and the learned parameters are then applied to quantum computations to improve performance.

Another related method involves optimizing the initial states of quantum circuits using classical tensor networks [35]. Although this approach appears similar to classical-quantum transfer learning, it focuses only on the initial state. In high-dimensional quantum computation [36], the limitations of the expressive power and high computational costs of tensor networks limit the tuning process to only these initial states. Conversely, in the classical-quantum transfer learning configuration of DUOM, any internal parameters can be learned by replacing QA with a classical and computationally cheap sampler. To the best of our knowledge, the proposed classical-quantum transfer learning algorithm is the first attempt at internal parameter tuning to reduce computational costs without using quantum computation in the training process.

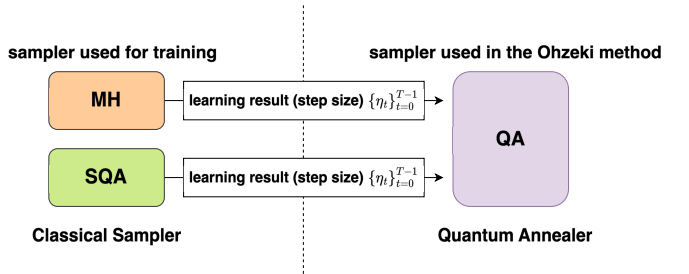


FIG. 2: Overview of classical-quantum transfer learning, where learned parameters using a classical sampler (left) are transferred to DUOM with a quantum annealer in execution (right).

V. EXPERIMENTS

In this section, we present numerical experiments conducted on an image reconstruction problem to verify the performance of classical-quantum transfer learning for DUOM. First, we focus on comparing MH with SQA, which approximates QA, as a classical sampler for training. Next, we examined the Trotter number in SQA, which controls the accuracy of the QA approximation. Finally, we compared the performance of DUOM with QA to that of a classical sampler during execution to analyze the effects of QA.

A. Problem and parameter settings

We focused on a two-dimensional binary image reconstruction using linear measurements. Let $\mathbf{x} \in \{0, 1\}^N$ be a vector representing a binary image of size $\sqrt{N} \times \sqrt{N}$. This problem aims to recover \mathbf{x} from the noiseless linear observations $\mathbf{y} = \mathbf{A}\mathbf{x}$, where $\mathbf{A} = (a_{kl})$ is an $M \times N$ random matrix ($M < N$) whose elements are independently drawn from a standard normal distribution. Assuming that the non-zero pixels in the original image are neighboring pixels, the problem is defined as

$$\min_{\mathbf{x} \in \{0, 1\}^N} - \sum_{\langle i, j \rangle} x_i x_j \text{ s.t. } y_k = \sum_{l=1}^N a_{kl} x_l \quad (k = 1, \dots, M), \quad (9)$$

where $\langle i, j \rangle$ denotes adjacent pixel pairs in the image. This formulation corresponds to Eq. (1) with $f_0(x) = -\sum_{\langle i, j \rangle} x_i x_j$, $f_k(x) = \sum_{l=1}^N a_{kl} x_l$, and $C_k = y_k$ for $k = 1, \dots, M$.

In the experiment, we set $N = 15^2 = 225$ and $M = 135$. The ratio $M/N = 0.6$ is lower than the statistical-mechanical threshold $M/N = 0.633$ [37]. It suggests that the COP is typically hard to solve in the thermodynamic limit ($N \rightarrow \infty$).

To implement unsupervised learning for DUOM, we generated datasets consisting of random matrices \mathbf{A} and corresponding observations $\mathbf{y} = \mathbf{A}\mathbf{x}^*$, with the original image \mathbf{x}^* fixed throughout the experiments, as illustrated in Fig. 3. In each parameter update, we used 20 mini-batches of size 4. The parameters $\{\eta_t\}_{t=0}^{T-1}$ were optimized using the Adam optimizer [31] to minimize the loss function in Eq. (2) of $\lambda = 1$.

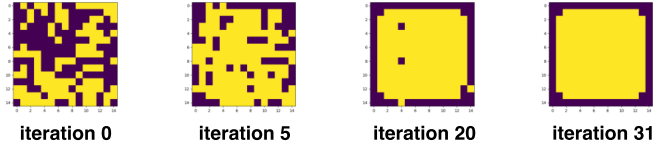


FIG. 3: Examples of reconstructed images using the Ohzeki method with $\eta = 1.0 \times 10^{-2}$. In each image of size 15×15 , yellow and purple represent $x_i = 1$ and $x_i = 0$, respectively. From left to right, the images correspond to iterations 0, 5, 20, and 31, where the rightmost image is equivalent to the original one.

The initial learning rate was set to 5.0×10^{-2} and was decayed by a factor of 0.8 at each iteration to enhance convergence. Incremental learning techniques [38] were applied to prevent the gradient vanishing. The total number of iterations was set to $T = 30$, with initial parameter values of $\eta_t = 1.0 \times 10^{-2}$ for all t .

To implement SQA, we used SQASampler from OpenJij [39], with the Trotter number set to the default value of 4 layers, unless otherwise noted. For comparison, the DUOM using MH was trained and executed under the same conditions defined in the previous study [13]. We used the Advantage-system 6.4 of the D-Wave machine as a quantum annealer.

B. Numerical results

1. Performance of DUOM with quantum annealer

First, we evaluated the performance of classical-quantum transfer learning. We compared three methods that uses QA in their execution: DUOM trained using SQA (SQA-QA), DUOM trained using MH (MH-QA), and the original Ohzeki method with a constant step size was optimized by a grid search.

Figure 4 illustrates performance results of these methods in terms of MSE. At each iteration, we computed the best MSE obtained from the sampler’s outputs and then averaged these values over 50 random instances. The same instances were used consistently throughout the numerical experiments. The error bars represent 95 percent confidence intervals of the data. These results indicated that the performance of SQA-QA, which transferred the training results from SQA to QA, achieved the highest performance, with MSE reaching zero within 30 iterations. In comparison, using a fixed step size without training did not reduce the MSE to zero within 50 iterations, indicating a significant performance improvement by classical-quantum transfer learning. Moreover, SQA-QA even outperformed MH-QA, which transferred the training results from MH to QA. This is possibly because SQA can approximate QA more accurately than MH, making the transfer learning to QA more effective. To examine this, we next com-

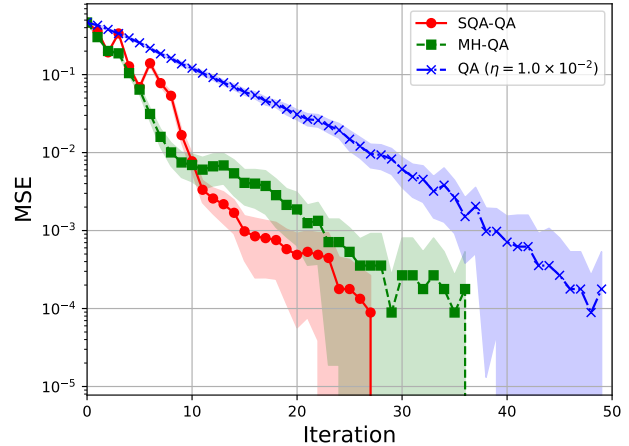


FIG. 4: MSE performance of DUOM by classical-quantum transfer learning as a function of the number of iterations. SQA-QA and MH-QA represent DUOM trained using SQA and MH, respectively.

pared the performance based on the Trotter number of SQA.

2. Trotter number dependency in SQA

SQA approximates QA by using multiple Trotter layers, as introduced by the Suzuki-Trotter decomposition [40, 41]. The Trotter number τ is a hyperparameter that controls the accuracy of the approximation. Given a limit of $\tau \rightarrow \infty$, SQA reproduces the original quantum system described by the Schrödinger equation, as required by the Suzuki-Trotter formula [40, 41]. However, it is important to note that the dynamics of SQA do not fully replicate the physical dynamics of QA, which are governed by the Schrödinger equation [42].

We conducted numerical experiments to examine the effect of the Trotter number on classical-quantum transfer learning. Figure 5 presents the numerical results when $\beta = \tau$. The MSE and the error bars are plotted in the same manner, as shown in Fig. 4. Note that SQA with $\beta = \tau = 1$ is equivalent to MH with the inverse temperature $\beta = 1$. In this case, the MSE failed to reach zero within 50 iterations, indicating poor performance. In contrast, when the Trotter number was increased to $\tau = 4$, DUOM achieved optimal solutions for all instances within 30 iterations. Increasing the Trotter number to $\tau = 8$ yielded nearly equivalent performance to that with $\tau = 4$, whereas optimal solutions were found by DUOM with fewer iterations for certain instances. This suggests that a large Trotter number in the SQA in the training process leads to better performance in classical-quantum transfer learning.

3. Comparison of quantum DUOM with classical DUOM

We now compare DUOM performance with different samplers used during execution. We considered three scenarios:

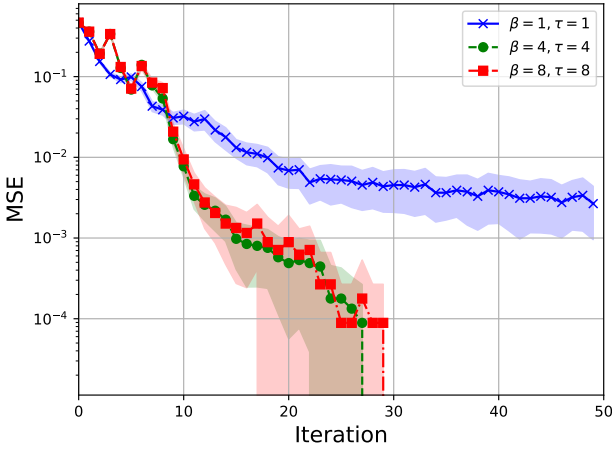


FIG. 5: Trotter number τ dependency of MSE performance for SQA-QA when $\beta = \tau$.

DUOM trained using SQA and executed on QA (SQA-QA), DUOM trained and executed using SQA (SQA-SQA), and DUOM trained and executed using MH (MH-MH). Note that SQA-SQA and MH-MH represent conventional classical DUOM configurations without transfer learning, whereas SQA-QA involved classical-quantum transfer learning.

Figure 6 presents the results of this experiment in terms of MSE. The MSE and the error bars are plotted in the same manner, shown as in Fig. 4. Here, the SQA-SQA method exhibited the best performance, with all instances converging to the optimal solutions within 15 iterations. In comparison, SQA-QA converged more slowly, requiring more iterations to obtain optimal solutions. The MH-MH exhibited the slowest convergence among them. The superior performance of SQA-SQA can be attributed to the consistency between the sampler used during training and execution. Because both the training and execution processes used SQA, the learned parameters were optimal for the SQA sampler. In contrast, SQA-QA involves transfer learning, where the algorithm used during training process differs from that used during execution. This discrepancy may lead to suboptimal performance compared to the SQA-SQA configuration.

We also examined execution time as another important metric for evaluating COP solvers. Specifically, we compared the three methods in terms of the execution time. Table I summarizes the average execution times required to solve a single instance. This table includes the average sampling time, gradient descent time, total execution time without an API, API response time for D-Wave, and the total execution time. Despite requiring more iterations, SQA-QA was significantly faster in terms of the total execution time than SQA-SQA. When the API response time was ignored, the execution time of SQA-QA was approximately 190 times faster than that of SQA-SQA. In particular, the sampling time of SQA-QA was negligible compared to that of SQA-SQA, whose execution time was dominated by the SQA sampler. Even if the API response time is considered, the total execution time for SQA-QA was

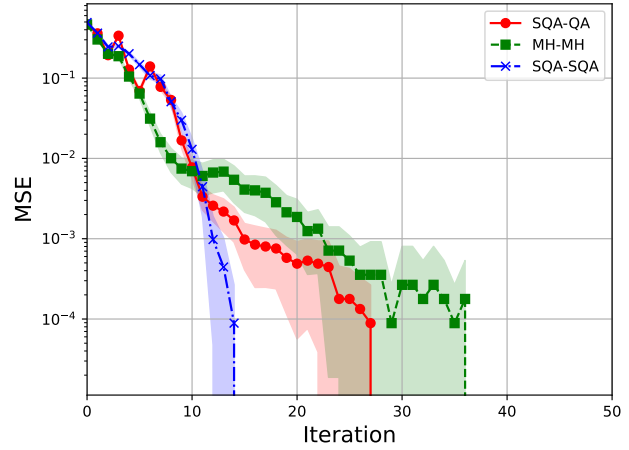


FIG. 6: MSE performance of DUOM by classical-quantum transfer learning (SQA-QA) with classical DUOM with MH (MH-MH) and SQA (SQA-SQA).

	Sampling	GD	Total w/o API	API	Total
SQA-QA	181 ms (53.1 ms)	108 μ s (32.9 ns)	181 ms (53.1 ms)	12.2 s (4.14 s)	12.2 s (4.14 s)
SQA-SQA	34.8 s (4.44 s)	180 μ s (43.3 ns)	34.9 s (4.44 s)	—	34.9 s (4.44 s)

TABLE I: Average (upper) and standard deviation (lower) of execution time for SQA-QA and SQA-SQA.

12.2 seconds, whereas that for SQA-SQA was 34.9 seconds. Although SQA-SQA converges in fewer iterations, the rapid sampling capability of the quantum annealer in SQA-QA significantly reduces the total execution time. This speed-up highlights the practical advantage of using a quantum annealer for execution, even when employing transfer learning. These results demonstrate that classical-quantum transfer learning can leverage the speed of quantum hardware to accelerate optimization, despite potential performance differences in convergence behavior.

VI. CONCLUSION

In this study, we proposed a novel trainable COP solver that integrates QA with DU using classical-quantum transfer learning. This approach effectively mitigates the high training costs associated with quantum computation by leveraging classical computation, thereby making quantum computation more accessible and efficient for deep-unfolded quantum algorithms. The results of numerical experiments on the image reconstruction problem demonstrated the practical viability and effectiveness of the proposed method. Specifically, the transfer learning approach, wherein step sizes are learned using a classical sampler and transferred to a quantum annealer,

showed a significant improvement in convergence speed and accuracy. Classical-quantum transfer learning is a classical-quantum hybrid method designed for trainable quantum algorithms.

The results highlighted the effect of using classical samplers such as MH and SQA, for training. The comparisons revealed that SQA, which better approximates QA, achieved superior performance when its training parameters were transferred to a quantum annealer. This indicates that selecting an appropriate classical sampler is crucial for effective classical-quantum transfer learning. In addition, the influence of the Trotter number in SQA on the accuracy of QA approximations was examined, showing that larger Trotter numbers improved the performance of classical-quantum transfer learning. This opens up new avenues for exploring different classical approximations to enhance learning efficiency.

Furthermore, the comparisons between classical and quantum DUOM demonstrated that although SQA-SQA requires

fewer iterations to converge compared to SQA-QA, the latter achieved a clear advantage in terms of execution time, emphasizing the practical utility and speed of quantum execution following training. These findings underscore the feasibility of deploying quantum-enhanced solvers trained on classical systems for real-world optimization tasks.

Future research directions include the following. First, it is crucial to verify the effectiveness of classical-quantum transfer learning and quantum DUOM for more practical problems, including the traveling salesman and graph partitioning problems. The application of this approach to COPs with inequality constraints, such as the knapsack problem [43], is another crucial area for further investigation.

ACKNOWLEDGMENTS

This study was partially supported by JSPS KAKENHI with Grants No. 22H00514 and No. 22K17964.

-
- [1] S. A. Cook, “The Complexity of Theorem-Proving Procedures,” in *Proceedings of the Third Annual ACM Symposium on Theory of Computing* (ACM, New York, 1971), pp. 151–158.
- [2] S. Kirkpatrick, C. D. Gelatt, and M. P. Vecchi, *Science* **220**, 671 (1983).
- [3] T. Kadowaki and H. Nishimori, *Phys. Rev. E* **58**, 5355 (1998).
- [4] V. S. Denchev, S. Boixo, S. V. Isakov, N. Ding, R. Babbush, V. Smelyanskiy, J. Martinis and H. Neven, *Phys. Rev. X* **6**, 031015 (2016).
- [5] D-Wave Systems Inc., <https://www.dwavesys.com>.
- [6] V. Choi, *Quant. Inf. Proc.* **7**, 193 (2008).
- [7] V. Choi, *Quant. Inf. Proc.* **10**, 343 (2001).
- [8] C. Klymko, B. D. Sullivan, and T. S. Humble, *Quantum Information Processing* **13**, 709 (2014).
- [9] W. Vinci, T. Albash, G. Paz-Silva, I. Hen, and D. A. Lidar, *Phys. Rev. A* **92**, 042310 (2015).
- [10] M. Ohzeki, *Sci. Rep.* **10**, 3126 (2020).
- [11] R. L. Stratonovich, *Sov. Phys. Dokl.* **2**, 416 (1957).
- [12] J. Hubbard, *Phys. Rev. Lett.* **3**, 77 (1959).
- [13] R. Hagiwara and S. Takabe, *J. Phys. Soc. Jpn.* **93**, 063801 (2024).
- [14] K. Gregor and Y. LeCun, “Learning Fast Approximations of Sparse Coding,” in *Proceedings of the 27th International Conference on Machine Learning* (Omnipress, 2010), pp. 399–406.
- [15] J. R. Hershey, J. Le Roux, and F. Weninger: Deep Unfolding: Model-Based Inspiration of Novel Deep Architectures; [arXiv:1409.2574](https://arxiv.org/abs/1409.2574)
- [16] S. Takabe and T. Wadayama, *IEICE Transactions on Fundamentals of Electronics, Communications and Computer Sciences*, **105**, 1110 (2022).
- [17] A. Balatsoukas-Stimming and C. Studer, “Deep Unfolding for Communications Systems: A Survey and Some New Directions,” in *Proceedings of the 2019 IEEE International Workshop on Signal Processing Systems* (IEEE, 2019), pp. 266–271.
- [18] D. Ito, S. Takabe, and T. Wadayama, *IEEE Trans. Signal Process.* **67**, 3113 (2019).
- [19] K. Zhang, L. Van Gool, and R. Timofte, “Deep Unfolding Network for Image Super-Resolution,” in *Proceedings of the IEEE Conference on Computer Vision and Pattern Recognition* (IEEE, 2020), pp. 3217–3226.
- [20] S. Takabe and T. Abe, *IEEE Wireless Commun. Lett.* **13**, 701 (2024).
- [21] S. Takabe, [arXiv:2306.16264](https://arxiv.org/abs/2306.16264) (2023).
- [22] S. Arai and S. Takabe, [arXiv:2408.03026](https://arxiv.org/abs/2408.03026), accepted to *Phys. Rev. Res.* (2024).
- [23] N. Metropolis, A. W. Rosenbluth, M. N. Rosenbluth, A. H. Teller and E. Teller, *J. Chem. Phys.*, **21**, pp. 1087–1092 (1953).
- [24] W. K. Hastings, *Biometrika* **57**, 97 (1970).
- [25] E. Crosson and A. W. Harrow, “Simulated Quantum Annealing Can Be Exponentially Faster than Classical Simulated Annealing,” in *Proceedings of the 57th Annual IEEE Symposium on Foundations of Computer Science* (IEEE, 2016), pp. 714–723.
- [26] G. E. Santoro, R. Martonák, E. Tosatti, and R. Car, *Science* **295**, 2427 (2002).
- [27] F. Glover, G. Kochenberger, R. Hennig, and Y. Du, *Ann. Oper. Res.* **314**, 141 (2022).
- [28] V. Monga, Y. Li, and Y. C. Eldar, *IEEE Signal Process. Mag.* **38**, 18 (2021).
- [29] N. Shlezinger, Y. C. Eldar, and S. P. Boyd, *IEEE Access* **10**, 115384 (2022).
- [30] S. Takabe and T. Wadayama, *IEICE Trans. Fundam. Electron. Commun. Comput. Sci.* **E105-A**, 1110 (2022).
- [31] D. P. Kingma and J. Ba, [arXiv:1412.6980](https://arxiv.org/abs/1412.6980) (2017).
- [32] PyTorch, <https://pytorch.org>.
- [33] K. Blekos, D. Brand, A. Ceschini, C. H. Chou, R. H. Li, K. Pandya, and A. Summer, *Phys. Rep.* **1068**, 1 (2024).
- [34] D. Wierichs, J. Izaac, C. Wang, and C. Lin, *Quantum* **6**, 677 (2022).
- [35] J. Dborin, F. Barratt, V. Wimalaweera, L. Wright, and A. G. Green, *Quantum Sci. Technol.* **7**, 035014 (2022).
- [36] G. Evenbly and G. Vidal, *J. Stat. Phys.* **145**, 891 (2011).
- [37] T. Tanaka, *IEEE Trans. Inf. Theory* **48**, 2888 (2002).
- [38] S. Takabe, M. Imanishi, T. Wadayama, and K. Hayashi, *IEEE Access* **7**, 93326 (2019).
- [39] OpenJij, <https://www.openjij.org/>
- [40] H. F. Trotter, *Proc. Am. Math. Soc.* **10**, 545 (1959).

- [41] M. Suzuki, *Commun. Math. Phys.* **51**, 183 (1976).
- [42] Y. Bando and H. Nishimori, *Phys. Rev. A* **104**, 022607 (2021).
- [43] S. Yu and T. Nabil, *Front. Phys.* **9**, 659463 (2021).